Fusion Engineering and Design 139 (2019) 155–162

Contents lists available at ScienceDirect

Fusion Engineering and Design

journal homepage: www.elsevier.com/locate/fusengdes

Optimization of the geometric parameters of the EAST articulated maintenance arm (EAMA) with a collision-free workspace determination in EAST

Kun Wang[a,b,c], Qi Wang[a,*], Yong Cheng[a], Huapeng Wu[c], Yuntao Song[a,b], Vincent Bruno[a,1]

[a] Hefei Institutes Of Physical Science, Chinese Academy of Sciences, Hefei, 230031, China
[b] University of Science and Technology of China, Hefei, 230026,China
[c] Lappeenranta University of Technology, Lappeenranta, Finland

ARTICLE INFO

Keywords:
EAMA
Geometric parameters
Coverage ratio
Monte carlo method
Workspace
Collision detection

ABSTRACT

An EAST Articulated Maintenance Arm (EAMA), upgraded based on an articulated inspection arm (AIA), which was successfully operated in Tore Supra in 2008, was developed for the purpose of the inspection and maintenance of damaged internal components during plasma discharges without breaking the East Advanced Superconducting Tokamak (EAST) ultra-high vacuum condition. However, the coupling structure and high redundancy of the EAMA, due to the requirement of coverage ratio and the limitation of the EAST environment, produces a limited accuracy in positioning control. Therefore, the optimal design of the geometric parameters plays a vital role in the EAMA's performance. In this paper, the main characteristics of the EAMA system are investigated to formulate the optimization into a multi-objective problem. Furthermore, an approach based on the Monte Carlo method, integrated with a dedicated collision detection algorithm in the EAST environment, is elaborated on, which is utilized to calculate the collision-free workspace of the EAMA. With the knowledge of the workspace, the coverage ratio is obtained by a progressive meshing technique. Finally, several groups of geometric parameters are sampled to calculate the corresponding value of the objective functions, and the optimized combination of the geometric parameters is obtained by comparing the results.

1. Introduction

Per the requirement of the higher operation parameters of EAST, the inner components of the first wall will be facing increasing heat and electromagnetic load [1]. Many different kinds of failures of the internal parts were found in practical experiments. Therefore, it is essential for timely maintenance based on the condition of damaged internal components in the experimental period [2]. Inspired by the articulated inspection arm (AIA), which was constructed in CEA-IRFM for visual inspection inside the Tore Supra Tokamak [3], the EAST articulated maintenance arm (EAMA) system was collaboratively developed by ASIPP and CEA-IRFM [1] for the purpose of the inspection and maintenance of damaged internal components during plasma discharges without breaking the EAST ultra-high vacuum condition. However, due to the limitation of the EAST environment, as shown in Fig. 1, the EAMA is designed as a snake robot with a highly redundant articulated series mechanism and several modules in order to avoid obstacles and further satisfy the requirements of the coverage ratio, which is the volume ratio between the workspace of the EAMA and the EAST vacuum vessel. Due to the mechanical characteristic of the EAMA, the structure flexibilities result in a bad performance of the positioning control [4], which can be mitigated by modelling the deflection and decreasing the length or number of EAMA modules. Therefore, there is a trade-off between the coverage ratio and flexibility of the EAMA, which can be conveniently conceived as a two-objective optimization problem.

It is clear that the workspace determination of a robot manipulator, which has been studied for more than three decades, is essential for computing one of the two objective functions, namely, coverage ratios. Many algorithms have been proposed for determining the workspace of the robot manipulator, including graphical, analytical and numerical methods. Zhongfei Wang, Shiming Ji et al. [5] presented a graphical method called the maximal regular-shaped dexterous workspace (MRsDW) method, which is based on the stratified workspace boundary

* Corresponding author.
E-mail address: wangqi8@ipp.ac.cn (Q. Wang).
[1] French Atomic Energy and alternative energy commission.

https://doi.org/10.1016/j.fusengdes.2019.01.033
Received 17 September 2018; Accepted 7 January 2019
Available online 19 January 2019
0920-3796/

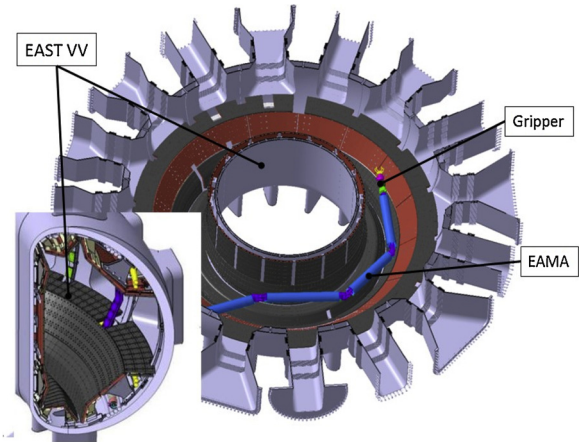

Fig. 1. Cross-section of the EAMA in the EAST vacuum vessel.

search technique. Yunfeng Wang et al. [6] proposed using the diffusion-based algorithm for workspace generation of hyper-redundant manipulators. The authors of [7] presented an analytical method called the collision-free force closure workspace (CFFCW) determination for reconfigurable planar cable-driven parallel robots (RPCDPRS). Central to this method is the determination of the collision-free area based on the RPCDPRS. However, these methods are dedicated and non-portable.

The Monte Carlo method is a numerical method for solving mathematical problems by means of random sampling [8]. In principle, the Monte Carlo method can be used to solve any problem that has a probabilistic interpretation. Unfortunately, the EAMA is a highly redundant manipulator with a narrow circumstance; therefore, the workspace of the EAMA is difficult to determine due to the large sampling time, which is caused by the large number of joints, and most of the sampled configurations of the EAMA are under collision with its environment, which should be filtered out from the workspace. In this paper, a geometry approach to detect the collision of each modular arm integrated with Monte Carlo methods is proposed to quickly and efficiently determine the workspace of the EAMA. The paper starts with an introduction in section 1 and then the EAMA system, basic configuration of the EAMA and optimization objectives are described in Section 2. Section 3 presents methods for dedicated collision detection in the EAST environment and the collision-free workspace determination, while Section 4 elaborates the results among several groups of geometric parameters. Finally, the conclusions are given in Section 5.

2. Problem description

This section describes the main characteristic of the EAMA system and the basic configuration to be used in the two-objective optimization problem. Finally, the two objective functions are formulated.

2.1. Description of the EAMA system

The EAMA system is composed mainly of a highly redundant snake-like robot named the EAMA and a storage cask (including several condition maintaining systems), as depicted in Fig. 2. The storage cask is used to generate a 10^{-5} Pa vacuum condition and push the EAMA into a vacuum vessel via a stainless shuttle.

The EAMA robot of the system adopted a modular design, and each module consists of a parallelogram mechanism, where four bars consist of a horizontal rod, robot tube, and two clevises. The mechanism provides two orthogonal degrees of freedom (DOFs), as shown in Fig. 3.

Among a set of specialized end-effectors, a dexterous gripper with 3 DOFs is mounted at the end of the EAMA for the tasks of grasping and inspection.

The basic configuration of the EAMA, as illustrated in Fig. 4, is composed of two kinds of modules. The module in blue is integrated with a light yaw joint actuator to provide the rotation motion, and the module in red is the same, as depicted in Fig. 3. The module in red can provide two kinds of motion: rotation and elevation. The configuration is adopted based on the requirements and characteristics of the mechanism listed below:

1 The modules in blue actuate the EAMA to rotate around the EAST vacuum vessel, and the modules in red can carry the end-effector to reach the horizontal planes at different altitudes.
2 As shown in Fig. 5 (a), a module that is longer than 1750 mm (calculated based on the size of the EAST environment) cannot be shuttled into the EAST vacuum vessel. Furthermore, considering the size of the EAST vacuum vessel, as shown in Fig. 5 (b), and the limit of the elevation motion ($\pm 45^\circ$ in the vertical plane), the basic configuration is constructed with two red modules.
3 The modules in red placed at the extremity of the EAMA help reduce the size of the actuators used to elevate the robot.

Therefore, the geometric parameters to be optimized are as follows: the numbers of modules, N, and the lengths of the two kinds of modules, L_1 and L_2.

2.2. Optimization objectives

The optimization of the geometric parameters is formulated as a multi-objective problem. There are two objectives that need optimization: (a) maximize the coverage ratio, and (b) minimize the flexibilities of the EAMA. As mentioned in Section 1, the workspace is essential for computing the coverage ratio, and the workspace boundary curve is composed of a series of line segments by connecting the boundary points [9]. Furthermore, as proposed in [10], the volume of the workspace can be calculated based on the progressive meshing technique. Therefore, the coverage ratio is evaluated as:

$$CR = \frac{V_{Workspace}}{V_{VacuumVessel}} \tag{1}$$

where $V_{Workspace}$ is the volume of workspace, $V_{VacuumVessel}$ is the volume of the EAST vacuum vessel, and CR is the coverage ratio. The approach for determining the workspace will be presented in section-3.

The flexibilities of a long-reach manipulator were theoretically analysed and modelled by J. Chalfoun in [4]. Due to its large dimension and redundant mechanism, a long-reach manipulator, such as the EAMA, contains many flexibilities. To model these flexibilities, J. Chalfoun and co-authors analysed gravity forces repartition in the parallelogram structure, as shown in Fig. 6, and created a flexible model with eight springs.

The tensions created in the parallelogram structure can be evaluated as [4]:

$$\begin{aligned} T_1 &= \frac{C}{l * \cos\alpha} \\ T_2 &= P * \frac{d}{l_1} \\ T_3 &= k_{t1} * DL = \frac{C}{l * \cos\alpha} + P\frac{L}{l_1} \end{aligned} \tag{2}$$

where α represents the elevation angle, k_{t1} denotes the spring with stiffness that represents the flexibility of the tube, and DL denotes the elastic deformation that is caused by tension T_3.

In this paper, we only consider the flexibilities that are related to the geometric parameters. They are formulated under the aligned state of the EAMA such that:

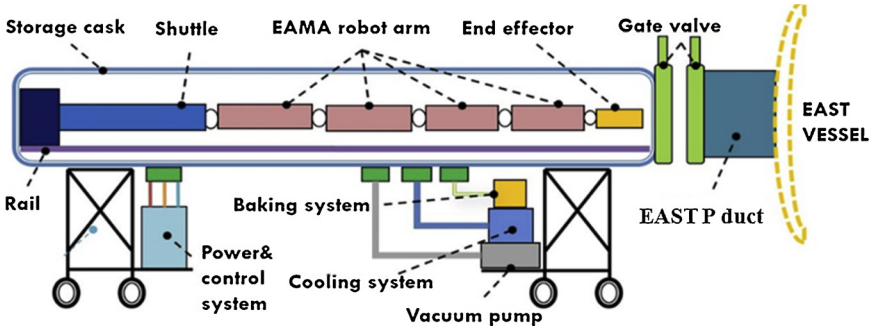

Fig. 2. Overall schematic view of the EAMA system.

$$DL2_i = {}^{T_3}/_{k_{t1}} = C_2{*}P2_i{*}L_2 + B_2$$
$$DL1_i = {}^{T_3}/_{k_{t1}} = C_1{*}P1_i{*}L_1 + B_1$$
$$P2_i = P2_{i+1} + G_2$$
$$P1_i = P1_{i+1} + G_1$$
$$G_2 = g_2{*}L_2$$
$$G_1 = g_1{*}L_1$$
$$D_{Total} = \sum_{i=1}^{N} DL2_i + \sum_{i=1}^{2} DL1_i = \frac{(1+N)N}{2}{*}g_2{*}C_2{*}L_2^2 + 3{*}C_1{*}g_1{*}L_1^2 \quad (3)$$

where DL2 and DL1 are the deformation of the blue and red module as shown in Fig. 4, respectively, $P2_i$ and $P1_i$ are the total weights that follow a specific module-i, G_1 and G_2 are the weights of the two kinds of modules, g_1, g_2, C_1, C_2, B_1 and B_2 are constant coefficients that are independent of the geometric parameters, and D_{Total}, used to represent the flexibilities, is the summation of the EAMA's deformation.

Hence, an overall multi-objective function F is defined as:

$$\max F(L_1,L_2,N) = CR(L_1,L_2,N)/\, D_{Total}\,(L_1,L_2,N) \quad (4)$$

where L_1, L_2 and N are the geometric parameters as depicted in Fig. 4 and F is subject to:

$$1250mm \le L_1 \le 1700mm,\ 1115mm \le L_2 \le 1500mm,\ N = 2or3$$

3. Approach for determining the workspace

The focus here is to deduce an algorithm for rapid collision detection and filter out the unreasonable configurations during sampling of the Monte Carlo method. Specifically, random sampling from the shuttle to the last module (module N + 2) and checking the collision state of every module to screen out the colliding configurations. Eventually, the workspace of the EAMA is determined, which is a set of end-points under all the collision-free states, and the coverage ratio is calculated based on the progressive meshing technique. The main advantages of the method utilized in the workspace determination of the EAMA are:

- The predictability, i.e., since the Monte Carlo sampling configurations are under collision conditions, the proposed method can predetect the collision state of a module before the next sampling state.
- The dedicated collision detection algorithms for each module make the workspace calculation more efficient and faster.

3.1. Collision detection algorithm

As described in Fig. 2, the collision states of the EAMA include three situations:

- colliding with the storage cask;
- colliding with the EAST P-duct;
- colliding with the EAST vacuum vessel.

Due to the narrow space of the cask and P-duct, the EAMA can only move in a line in the cask, and the elevation movement is prohibited in the EAST P-duct. Therefore, the algorithm consists of two parts: finding the legal ranges of the yaw joint variables of a module in a P-duct under a given displacement of the shuttle and detecting the collision state of a module in the EAST vacuum vessel.

3.1.1. Legal ranges of a module in EAST P-duct

As the elevation motion is prohibited, determining the legal ranges of a module in the P-duct under a given displacement of the shuttle becomes a planar problem. Fig. 7 (a) shows two critical collision states of a module, where θ_1 and θ_2 denote the yaw joint variables of the two states, respectively. As depicted in Fig. 7 (b) and (c), critical state-I represents the state when the module contacts boundary wall-I of the EAST P-duct, and critical state-II includes two states: contact with boundary wall-II or the diagnostic device; thus, the legal ranges of a module in P-duct are an interval $[\theta_2, \theta_1]$. In practice, the module and the diagnostic devices are treated as two rectangles, and the boundary walls of the EAST P-duct are simplified into two lines; thus, θ_1 and θ_2 can be solved easily through their corresponding equations.

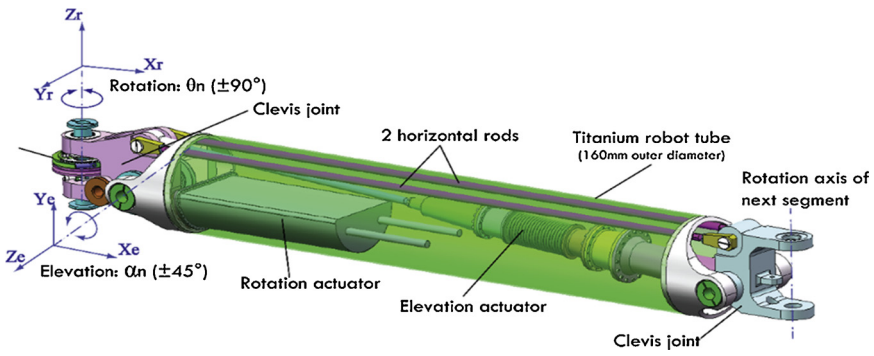

Fig. 3. Modular design of the EAMA robot arms.

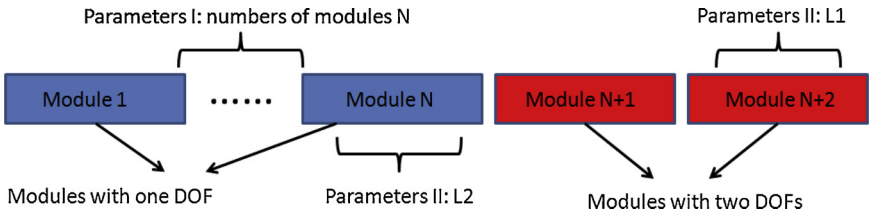

Fig. 4. Basic configuration of the EAMA.

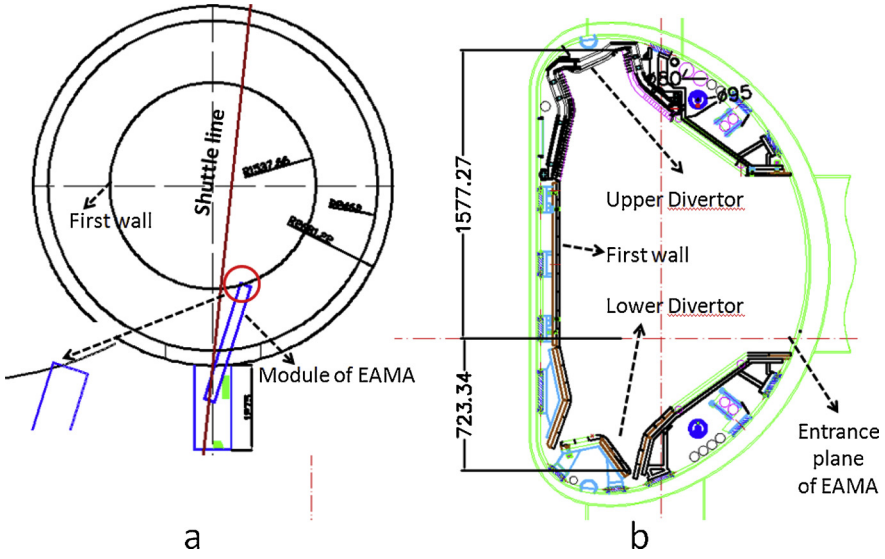

Fig. 5. Geometric size of the EAST vacuum vessel (VV): (a) Cross-section drawing of EAST VV, (b) Profile of EAST VV.

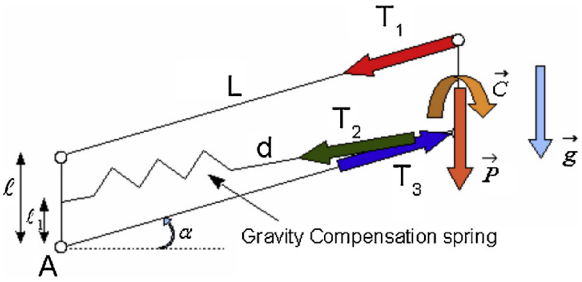

Fig. 6. Gravity forces repartition in the parallelogram structure of a module.

3.1.2. Collision detection of a module in the EAST vacuum vessel

To simplify the collision detection process, the EAST vacuum vessel is fitted by regular shadow objects, as shown in Fig. 8 (a). Additionally, all the faces of the vacuum vessel are extended along its radial direction, and the offset is equal to the radius of the tube in a module; thus, modules of the EAMA can be simplified into lines during collision detection between the EAMA and the vacuum vessel. Fig. 8 (b) shows a collision-free space in three dimensions that includes three kinds of faces: faces in red, blue and white, which belong to a cylinder, cone and an annulus, respectively. Therefore, the collision detection between a module of the EAMA and the vessel can be divided into two parts:

-
  -
    - Collision detection between a three-dimensional (3D) line-segment and the cylinder (the object in red);
    - Collision detection between a 3D line-segment and an object that is composed of a cone and an annulus.

3.1.2.1. Collision detection between a 3D line-segment and a cylinder. As illustrated in Fig. 9, line AB is the common perpendicular between the 3D line P_1P_2 and axis of the cylinder in red. Based on the relationship among these vectors, an equation can be obtained such that:

$$\overrightarrow{OA} + \overrightarrow{AB} + \overrightarrow{BP_1} = \overrightarrow{OP_1} \tag{5}$$

$$t_1 * vector_1 + t_2 * vector_2 + t_3 * vector_3 = \overrightarrow{OP_1} \tag{6}$$

$$[vector_1 \quad vector_2 \quad vector_3] * \begin{bmatrix} t_1 \\ t_2 \\ t_3 \end{bmatrix} = \overrightarrow{OP_1} \tag{7}$$

where $vector_1$ and $vector_2$ denote the directional vector of the axis of a cylinder and the common perpendicular, respectively. $Vector_3$ represents the vector from point1 to point2, and t_1, t_2 and t_3 represent the magnitude of corresponding vectors. Writing Eq. (5) into a matrix form will transform it into linear equations, as in Eq. (6), and t_1, t_2 and t_3 can be calculated by solving the equations. The normal distance between the 3D line and the axis of cylinder (magnitude of the common perpendicular) is evaluated as:

$$|\overrightarrow{AB}| = t_2 * |vector_2| \tag{8}$$

where $|\ |$ represents the norm operator of vectors. Apparently, it is necessary and sufficient to determine the relationship between the 3D line and the cylinder based on the magnitude of vector AB and the radius of the cylinder. However, there is a special state of a line-segment as shown in Fig. 9, where the 3D line collides with the cylinder when the normal distance is less than the radius of the cylinder. However, there is no interference between the line-segment P_1P_2 and the cylinder (Fig. 10).

The main procedure is summarized in the flowchart below:

3.1.2.2. Collision detection between a 3D line segment and the cone-annulus object. The free necessary and sufficient interference conditions between the 3D line and the cone-annulus body are such that:

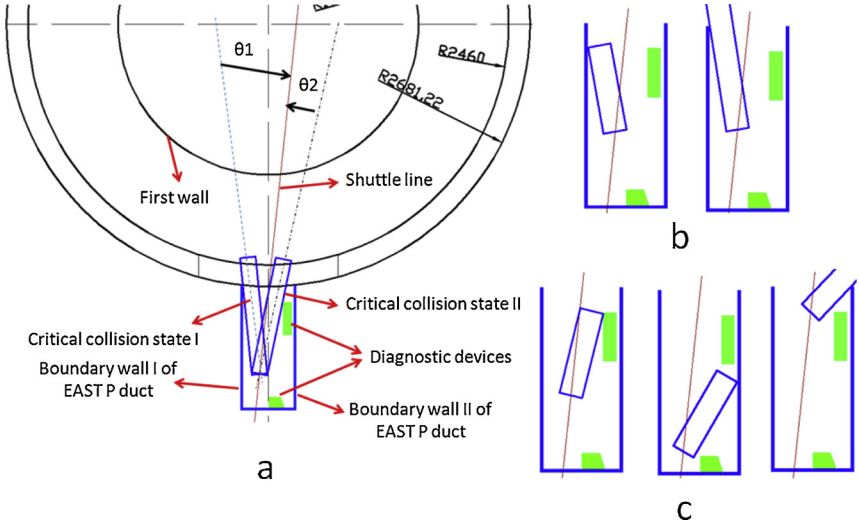

Fig. 7. (a). Critical collision states of a module with the EAST P-duct.
(b). Critical collision states of a module with boundary wall-I of the EAST P-duct.
(c). Critical collision states of a module with boundary wall-II of the EAST P-duct.

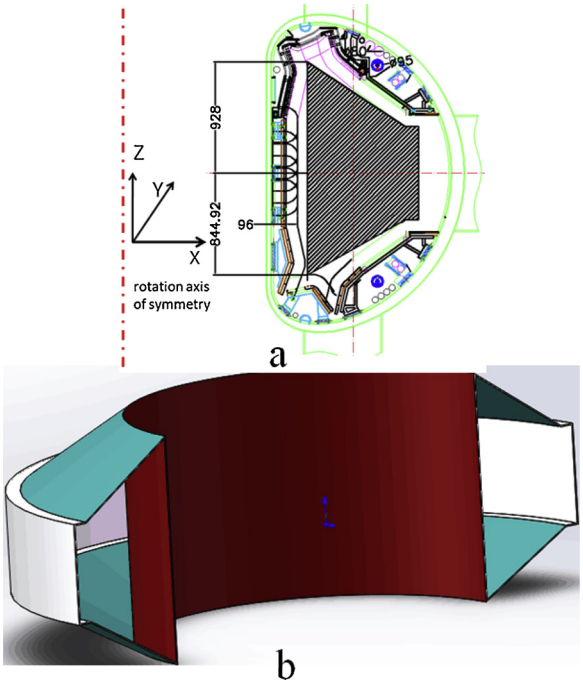

Fig. 8. Fitting primitives of the EAST vacuum vessel: (a) Profile of the fitting primitives, (b) Standard 3D view of the fitting primitives.

1 Two vertices of the 3D line segment are inside of the cone-annulus body;
2 The variation of pitch joint variable α is within [-θ, θ] as shown in Fig. 11.

Equations of the cone body in blue, as shown in Fig. 8, can be written as:

$$C_1 * (\sqrt{x^2 + y^2}) + C_2 * z + C_3 = 0 (C_1 < 0) \quad (9)$$

$$D_1 * (\sqrt{x^2 + y^2}) + D_2 * z + D_3 = 0 (D_1 < 0) \quad (10)$$

where C_1, C_2, C_3, D_1, D_2 and D_3 are constant coefficients.

Equations of the annulus body in white are as follows:

$$x^2 + y^2 = R_1^2 or x^2 + y^2 = R_2^2 (|z| < H) \quad (11)$$

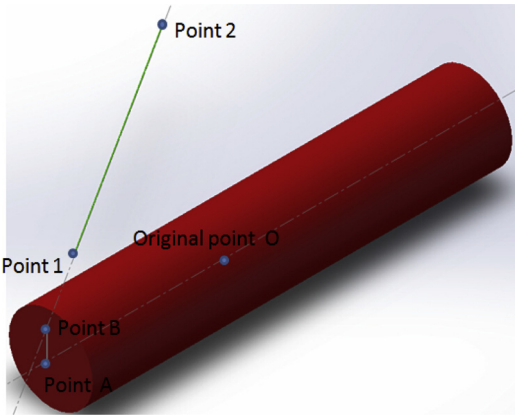

Fig. 9. A 3D line-segment and a cylinder.

where H is half of the height of the annulus, and R_1 and R_2 are the radiuses of the inner and outer circle, respectively, as described in Fig. 11 (b).

Assuming the two vertices of a line segment are point_1 (x_1, y_1, z_1) and point_2 (x_2, y_2, z_2), and taking point_1 for an example, the collision-free condition_1 should satisfy:

IF $R < \sqrt{x_1^2 + y_1^2} \le R_1$

$$D_1 * (\sqrt{x_1^2 + y_1^2}) + D_2 * z_1 + D_3 > 0 \quad (12)$$

$$C_1 * (\sqrt{x_1^2 + y_1^2}) + C_2 * z_1 + C_3 > 0 \quad (13)$$

ELSE IF $R_1 \le \sqrt{x_1^2 + y_1^2} < R_2$

$$|z_1| < H \quad (14)$$

Fig. 11 (a) depicts the critical collision state of the line segment and the connection interface of the cone and annulus, where Fig. 11 (b) is the projection of Fig. 11 (a), and α and θ denote the yaw joint and pitch joint variables, respectively. Equations with respect to the pitch joint variable θ can be expressed as:

$$S_2^2 - 2S_1S_2 * \cos(\alpha) + S_1^2 - R_2^2 = 0 \quad (15)$$

$$\tan(\theta) = \frac{S_3}{S_2} \quad (16)$$

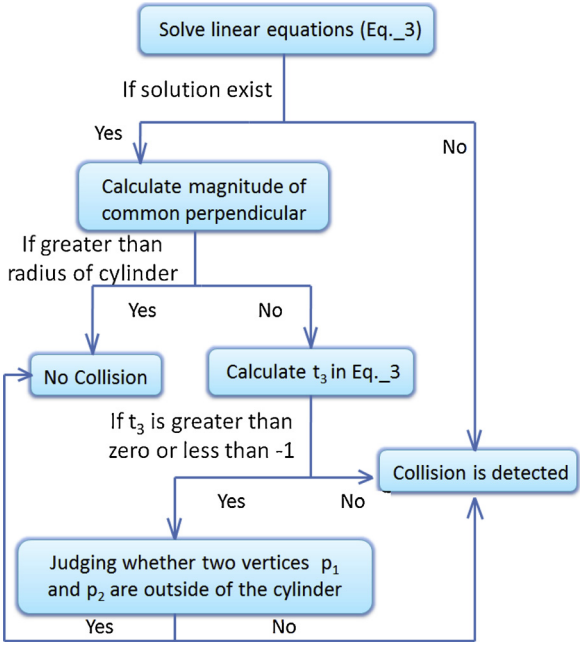

Fig. 10. Flowchart of collision detection between a 3D line-segment and a cylinder.

Clearly, condition_2 can be met when the pitch joint variable is in the range [-atan(S_3/S_2), atan(S_3/S_2)].

3.2. Workspace determination

After the collision detection algorithms are established, the approach for determining the workspace of the EAMA can be divided into two algorithms, as presented below.

Before the computation, the values of the geometric parameters (numbers of modules-N, length of the two modules L_1 and L_2, as shown in Fig. 4) must be optimized, and the maximum sampling times and the reference coordinates of Denavit-Hartenberg (D–H) models, as shown in Fig. 12, must be specified.

Algorithm A. Based on the Monte Carlo method, algorithm A consists of uniform random sampling for all the joints of the current module and checking the collisions for each sampled state. Specifically, the method calculates all the possibilities of the coordinates of the point that connect the current module and the following one and screens those out that are under the collision state. The steps of algorithm A are described below:

1 Input the coordinates of the connection point between a module and its antecedent and further judge the state of the module, which is in one three states: cask, EAST P-duct or EAST vacuum vessel.
2 If the module is in cask, set the variable of the yaw joint to its initial value.
3 If the module is inside of the EAST P-duct, use uniform random sampling in the legal range of the current state for the yaw joint, which is computed using the previous collision detection algorithm in Section 3.1.1.
4 If the module has two DOFs and is in the EAST vacuum vessel, use uniform random sampling in the intervals [-90deg, 90deg] and [-45deg, 45deg] for the yaw and pitch joints, respectively (for a module with only one DOF, only the yaw joint is sampled), and further judge the collision state.
5 Calculate and store the coordinates of the connection point between the module and its antecedent.
6 If the max cycle times are reached, then all the stored coordinates are outputted.

Algorithm-A is schematically illustrated in the block diagram in Fig. 13.

Algorithm B. Algorithm B determines the workspace of the EAMA by applying algorithm A to shuttle through the last module. The details are described below:

1 Use uniform random sampling to determine the displacement of the shuttle in the interval [0, 8000 mm].
2 Input the displacement of the shuttle into algorithm A and calculate all the possibilities of the coordinates of O_1, as shown in Fig. 12.
3 Input one of the possibilities of O_1 into algorithm A to calculate all the possibilities of O_2.
4 Recursively calculate the coordinates of the following points until the end point-O_{N+3}, as shown in Fig. 12, is obtained and stored as an element in the workspace clouds.
5 Repeating step 3 for all the possibilities.
6 Output the workspace clouds consisting of all points to define the workspace of the EAMA.

The main procedure of algorithm B is summarized in Fig. 14.

With the two algorithms, the workspace of the EAMA is determined; thus, the overall function F can be calculated by substituting Eqs. (1) and (3) into Eq. (4).

4. Simulations and discussion

The geometric parameters are sampled in the range discussed in Section 2 to obtain the most appropriate combination by comparing their performances in the overall function F. The geometric parameters L_1 and L_2 are sampled every 100 mm and 85 mm, respectively. N is chosen between number two and three. Fig. 15 shows the results among these parameter combinations.

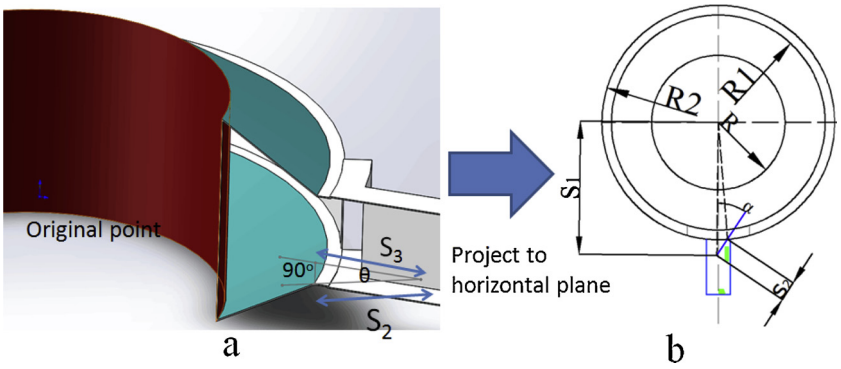

Fig. 11. Critical collision state of an elevation module.

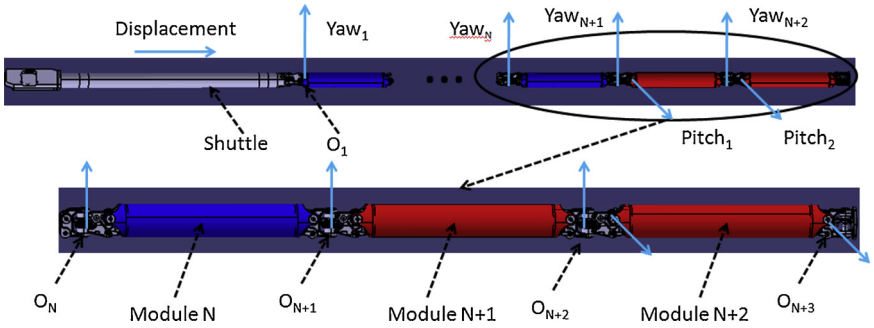

Fig. 12. D–H coordinates of the basic configuration of the EAMA.

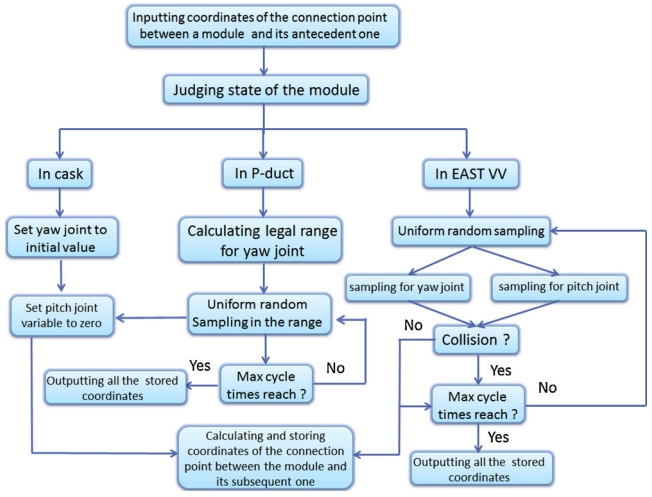

Fig. 13. Block diagram of algorithm A.

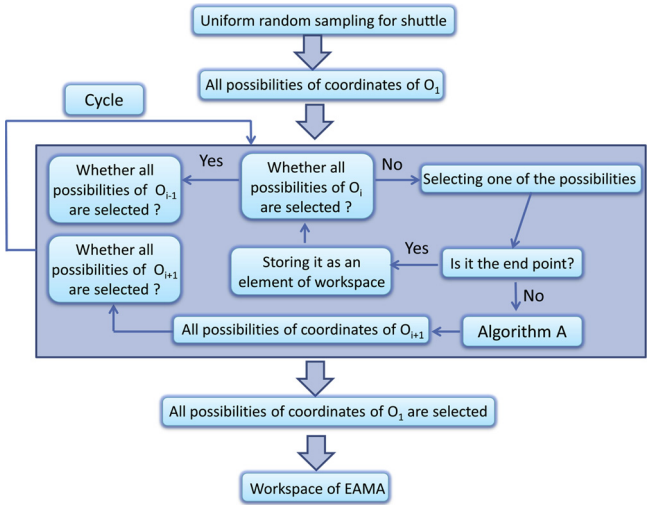

Fig. 14. Block diagrams of algorithm B.

Clearly, the optimized combination is that $L_1 = 1250$ mm, $L_2 = 1200$ mm and $N = 3$. Fig. 16 (a) and (b) show workspace clouds of the optimal solution in the front view and back view, respectively, where the blue points refer to the points of the workspace.

From Figs. 15 and 16 some features can be observed:

1 The objective function F holds a larger value of $N = 3$ than $N = 2$, which is caused by the fact that some areas are too narrow to approach with a smaller number of modules.
2 In principle, due to the narrow space of the EAST environment as discussed in Section 2, a small dimension of elevation modules (L_2) contribute to improving the dexterity of the EAMA in the range [1200 mm, 1700 mm].

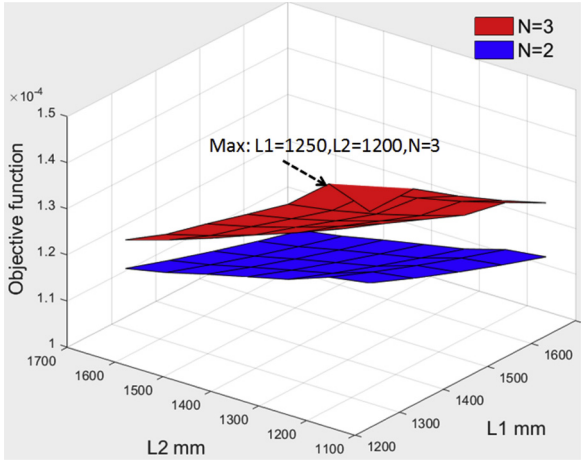

Fig. 15. Values of the objective function among the sampled groups of geometric parameters.

Additionally, some areas near the entrance are unreachable, as depicted in Fig. 17; therefore, it is impossible to achieve a one-hundred percent coverage ratio. Fortunately, the 3-DOF gripper, which is mounted at the end of the EAMA, can operate in these areas.

5. Conclusion

The optimization of geometric parameters plays a vital role in the optimal design of an EAMA. This paper formulates the optimization process as a multi-object optimization problem, where the object is to maximize the object function F with the following parameters: length L_1, L_2 and the number of modules N. A modified Monte Carlo geometry method is proposed for calculating one of the objective-coverage ratios among several groups of geometric parameters of the EAMA, and a dedicated collision detection algorithm based on the geometrical characteristics of the circumstance of the EAMA robot is derived to expedite the calculation. The computation results show that the optimal solution is as follows: $L_1 = 1250$ mm, $L_2 = 1200$ mm and $N = 3$.

Acknowledgements

This work was supported by the National "973" Program of China (Chinese ITER Special Support Project, No. 2014GB101000). We also deeply thank all the members of the EAMA design team, as well as the colleagues in ASIPP and CEA IRFM, for their hard work and beneficial discussions.

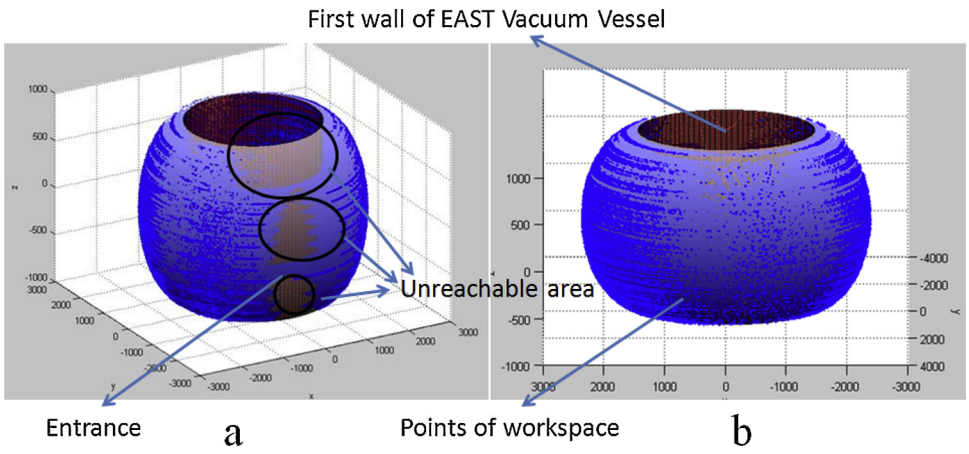

Fig. 16. Workspace clouds for the EAMA robot of the optimal solution; blue points represent the position where the EAMA can reach (Entrance of Port P is the only entry point for the EAMA robot) (For interpretation of the references to colour in this figure legend, the reader is referred to the web version of this article).

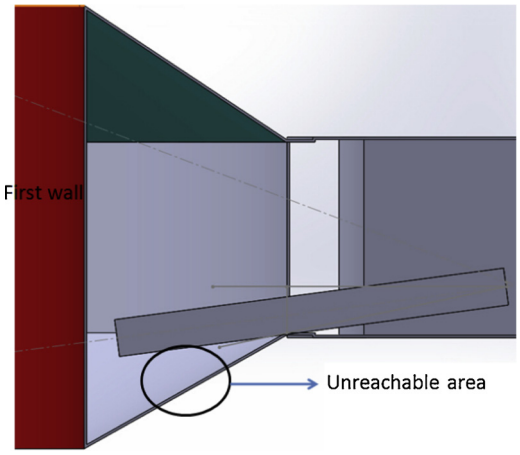

Fig. 17. Schematic of unreachable area of the EAMA in EAST VV.

References

[1] Shanshuang Shi, Yuntao Song, et al., Conceptual design main progress of EAST Articulated Maintenance Arm (EAMA) system, Fusion Eng. Des. 104 (2016) 40–45.
[2] Hongtao Pan, et al., Concetual design of EAST multi-purpose maintenance deployer system, Fusion Eng. Des. 118 (2017) 25–33.
[3] L. Gargiulo, et al., Operation of an ITER relevant inspection robot on Tore Supra tokamak, Fusion Eng. Des. 84 (2009) 220e223.
[4] J. Chalfoun, et al., Flexible modeling of a Long reach articulated carrier: geometric and elastic error calibration, IEEE International Symposium on Computational Intelligence in Robotics and Automation, (2007), pp. 321–326.
[5] Zhongfei Wang, Shiming Ji, A methodology for determining the maximal regular-shaped dexterous workspace of the PMs, 2007 IEEE International Conference on Mechatronics and Automation (2007) 827–832.
[6] Yunfeng Wang, Workspace generation of hyper-redundant manipulators as a diffusion process SE(N), IEEE Trans. Robot. Autom. 20 (3), June) (2004) 399–408.
[7] Bingyao Wang, Bin Zi, Collision Free force closure workspace determination of reconfigurable planar cable driven parallel robot, Asia-Pacific Conference on Intelligent Robot Systems, (2016), pp. 26–30.
[8] Yi Cao, Ke Lu, Xiujuan Li, et al., Accurate numerical methods for computing 2D and 3D robot workspace, Zang: accurate numerical methods for computing 2D and 3D robot workspace, Adv. Robotic Syst. 8 (6) (2011) Special Issue Robot Manipulators, 1-13.
[9] Tao Li, Hui Li, Marco Ceccarelli, Workspace determination of a chameleon-like space service robot with planar configurations, IEEE 5th International Conference on Robotics, Automation and Mechatronics (RAM), (2011), pp. 190–195.
[10] Tian Haibo, Workspace and Structural Parameters Analysis for Manipulator of Serial Robot, Transactions of the Chinese Society for Agricultural Machinery, 2013-04 (2019).